Bridge-Splitting Reactions of Platinum(II) Complexes with Parametalated Pyridine Spacer Groups: A Kinetic and Mechanistic Study

PETER O. ONGOMA, DEOGRATIUS JAGANYI

School of Chemistry and Physics, University of KwaZulu-Natal, Pietermaritzburg 3209, South Africa

Received 3 January 2013; revised 3 May 2013; accepted 22 May 2013

DOI 10.1002/kin.20806
Published online 23 July 2013 in Wiley Online Library (wileyonlinelibrary.com).

ABSTRACT: Substitution reactions of three dinuclear Pt(II) complexes connected by a pyridine-bridging ligand of variable length, namely [*cis*-{$PtOH_2(NH_3)_2$}$_2$–μ–L]$^{4+}$, where L = 4,4′-bis(pyridine)sulfide (**Pt1**), 4,4′-bis(pyridine)disulfide (**Pt2**), and 1,2-bis(4-pyridyl)ethane (**Pt3**) with S-donor nucleophiles (thiourea, 1,3-dimethyl-2-thiourea, and 1,1,3,3-tetramethyl-2-thiourea) and anionic nucleophiles (SCN^-, I^-, and Br^-) were investigated. The substitutions were followed under pseudo–first-order conditions as a function of the nucleophile concentration and temperature, using stopped-flow and UV–visible spectrophotometric methods. The observed pK_a values were, respectively, **Pt1** (pK_{a1}: 4.86; pK_{a2}: 5.53), **Pt2** (pK_{a1}: 5.19; pK_{a2}: 6.42), and **Pt3** (pK_{a1}: 5.04; pK_{a2}: 5.45). The second-order rate constants for the lability of aqua ligands in the first step decreased in the order **Pt2** > **Pt3** > **Pt1**, whereas for the second step it is **Pt1** > **Pt2** > **Pt3.** The obtained results indicate that introduction of a spacer atom(s) on the structure of the bridging ligand influences the substitution reactivity as well as acidity of the investigated dinuclear Pt(II) complexes. Also nonplanarity of the bridging ligand of **Pt1** complex significantly slows down the rate of substitution due to steric hindrance, whereas release of the strain enhances the dissociation of the bridging ligand. The release of the bridging ligand in the second step was confirmed by the ^{1}H NMR of **Pt1-Cl** with thiourea in DMF-d_7. The

Correspondence to: Deogratius Jaganyi; e-mail: jaganyi@ukzn.ac.za.

Contract grant sponsor: University of KwaZulu-Natal.
Contract grant sponsor: National Research Foundation, South Africa.
Contract grant sponsor: Egerton University, Kenya.
Supporting Information is available in the online issue at www.wileyonlinelibrary.com.

temperature dependence of the second–order rate constants and the negative values of entropies of activation ($\Delta S^{\#}$) support an associative mode of the substitution mechanism. © 2013 Wiley Periodicals, Inc. Int J Chem Kinet 45: 676–691, 2013

INTRODUCTION

Metal complexes are the main resources for the generation of chemical diversity, which includes novel Pt(II) anticancer therapeutic agents [1]. A number of Pt(II) anticancer agents, enjoying widespread use in the clinic, owe their anticancer activity to their ability to bind covalently or through intercalation of the aromatic ligands to cellular DNA. This alters the tertiary structure of DNA, resulting in the death of the cancer cell through apoptosis [2–6]. Although *cis*-diamminedichloridoplatinum(II) (*cis*platin) is one of the most active and clinically effective agents used in 50–70% of all cancer patients, especially against testicular, ovarian, head and neck carcinomas [7–9], the impetus to find new drugs stems from difficulties related to its use because of drug resistance and severe side effects [10]. However, systematic kinetic and mechanistic study of these complexes with relevant biological nucleophiles has not been fully explored to provide detailed insight into the kinetics and thermodynamic properties that control the lability (reactivity) of these complexes.

Over the past few years, many kinetic studies have aimed at tuning reactivity of the dinuclear Pt(II) complexes by altering their structures using a variety of different ligands [11,12], e.g., flexible α,ω-alkanediamines [13] or rigid azoles [14], and diazines [15,16], so as to modulate their reactivity toward nucleic acids and other biological nucleophiles in comparison with their mononuclear analogues. Two approaches have commonly been used to tailor the substitution process at the metal centers without changing the parent structure of the complex: control of their electronic properties by introducing a σ-donor and/or π-acceptor group or extending the π-conjugation [17–19] and by introducing steric hindrance around the Pt(II) center. Steric hindrance is observed for heterocycles containing one or two ortho groups, and these effects may be additive [20].

Against this background, several reports have indicated that bulky planar ligands such as pyridine and substituted pyridines attached next to the metal center in Pt(II) complexes, e.g., *cis*-$[PtCl(NH_3)_2$(2-methylpyridine)$]^+$ and *cis*-$[Pt(NH_3)_2Cl$(4-methylpyridine$]^+$ [21], could reduce the rate of reaction between the metal complexes and biomolecules containing –SH groups due to steric hindrance around the Pt(II) ion [6,22]. In recent reports, Jaganyi and his group [23] have studied the importance of introducing electron-donating methyl groups at 2,3-, 2,6-, and 2,5-positions of the pyrazine-bridging moiety and noted that increased steric hindrance and the σ-inductive effect decreased the positive charge on the metal center, slowing down reactivity of the Pt(II) complexes. In addition, recent studies [24–26] have established that there is a strong interaction between the two Pt(II) centers of dinuclear complexes, which proportionately weakens as the chain length and flexibility of the linker are increased. The other factors that influence reactivity of multinuclear Pt(II) complexes include hydrogen-bonding capacity, charge at the metal center and the linker, and the geometry of the leaving ligand relative to the linker [27–29].

We have systematically demonstrated that the *cis*-dinuclear Pt(II) complexes bridged by the diazine ligands [30] are degraded by thiourea, resulting in the loss of the integrity of the dinuclear structure and eventually releases the linker in contrast to what was reported by Farrell and coworkers [31]. This is due to the strong trans influence of the sulfur atom that weakens the am(m)ine nitrogen–platinum bond, making it susceptible to further substitution reactions [32].

Pyridine has extensively been used as a ligand for the synthesis of new platinum coordination compounds because of its ability to connect metal centers by forming metal-to-ligand bonds. To further our knowledge on the release of the bridging ligand that has been observed as partial or full degradation in a number of studies [21,33–35] but with very limited kinetic investigation, sp^3 hybridized sulfur spacer groups at the 4-position of the pyridine unit were investigated.

In this study, we report the kinetic and thermodynamic data for the substitution of the aqua ligand of the dinuclear Pt(II) complexes of the type $[\{cis\text{-}Pt(NH_3)_2(H_2O)\}_2L]^{4+}$ (L = 4,4′-bis(pyridine)sulfide or 1,2-bis(4-pyridyl)ethane) (Scheme 1), by thioureas (thiourea, TU; 1,3-dimethyl-2-thiourea, DMTU; and 1,1,3,3-tetramethyl-2-thiourea, TMTU) and ionic (Br^-, I^-, and SCN^-) nucleophiles. These complexes, especially S- or Se-based dinuclear complexes, have shown in vitro antitumor activities against cisplatin-sensitive L1210 (mouse leukemia) and cisplatin-insensitive HCT8 (human colodenocarcinomas) cell lines [36,37]. The pK_a values have also been determined for the two aqua ligands and together

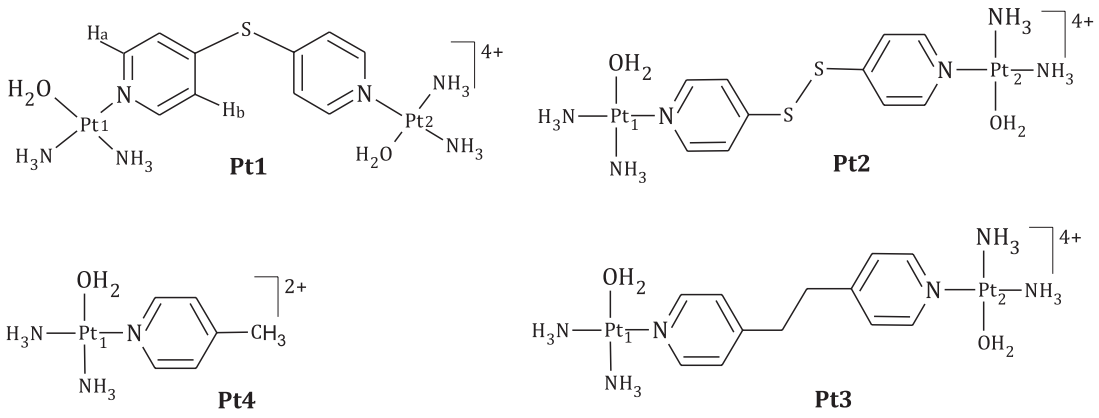

Scheme 1 Structures of the investigated dinuclear Pt(II) complexes. Included for comparison of pK_a and computation data purposes is the mononuclear complex **Pt4**. The numbering system adopted for the Pt centers is indicated on the structure of **Pt1**.

with the density functional theory (DFT) calculations interpreted to provide an insight into the factor(s), either electronic or structural effects that influence the ground state or transition state of the reaction.

EXPERIMENTAL

Materials

*Cis*platin (*cis*-($PtCl_2(NH_3)_2$; 99%) was purchased from Strem Chemicals. Methanol (Saarchem, Merck Chemicals, Wadeville, South Africa) was distilled over magnesium before use [38]. The nucleophiles TU (99%), DMTU (99%), TMTU (98%), sodium bromide (NaBr; 99%), sodium iodide (NaI; 99%), sodium thiocyanide (NaSCN; 99%), and the ligands: 4-mercaptopyridine (95%), 4,4′-dipyridyldisulfide (dpss; 98%), 1,2-bis(4-pyridyl)ethane (bpe; 99%), dipyridinium hydrochloride (98%), 4-bromopyridine hydrochloride (99%), sodium perchlorate monohydrate* ($NaClO_4.H_2O$; 98%), and perchloric acid ($HClO_4$; 70%) were obtained from Aldrich (Capital Lab Supplies CC, New Germany, South Africa) and used without further purification. Silver perchlorate ($AgClO_4$; 99.9%) from Aldrich was stored under nitrogen and used as supplied. Ultrapure water (Modulab Systems; Continental Water Systems, NSW, Australia) was used in all experiments.

Instruments and Measurements

Microanalyses were carried out on a Carlo Erba CHNS elemental analyzer 1106. Infrared spectra (KBr pellet, range 4000–300 cm^{-1}) were recorded on a Perkin Elmer Spectrum One-FTIR spectrophotometer. NMR spectra were acquired from a Bruker Avance DPX 500 instrument (^1H, 500 MHz) and (^{195}Pt, 107.5 MHz), respectively, at ambient temperature of 30°C. Values of ^1H are given in δ (ppm) relative to tetramethylsilane ($\delta = 0.00$), and ^{195}Pt the chemical shifts were externally referenced to $K_2[PtCl_4]$ in D_2O. Mass spectrometric analyses were collected on a Hewlett Packard LC–MS, using electron impact (EI) ionization. All pK_a titrations and kinetic and spectroscopic measurements for slower reactions were recorded on a Varian Cary 100 biospectrophotometer equipped with a thermostated cell holder. Kinetic measurements on fast substitution reactions were monitored using an Applied Photophysics SX 18 MV (v4.33) stopped-flow reaction analyzer coupled to an online data acquisition system. The temperature of instrument was controlled to within ±0.1°C. pK_a values, rate constants, and standard deviations were calculated using Microcal-origin version Origin-7.5® [39] software package.

Preparation of 4,4′-Dipyridylmonosulfide Ligand

The ligand 4,4′-dipyridylmonosulfide (dps) was prepared (Scheme S1 in the Supporting Information) using a slightly modified method previously described in the literature [40]. A mixture of 4-mercaptopyridine (1.8 g, 16.2 mmol), 4-bromopyridine (3.0 g, 15.4 mmol), and potassium carbonate (2.0 g) in dimethylformamide (15.0 mL) was kept under reflux at 120°C for 48 h. After the reaction was complete, the mixture was cooled and the crude product

*Metal perchlorate complexes and perchloric acid are potentially explosive. They should be handled with care, and the complexes should be prepared in small quantities.

was treated with water and then extracted with dichloromethane (5 × 20 mL).The organic layer was dried over anhydrous sodium sulfate. The solvent was evaporated under reduced pressure, and the residue purified by column chromatography on silica gel (eluent: hexane/ethyl acetate 7:1) to afford a yellow solid 4,4′-dipyridylmonosulfide. The purity of the isolated product was confirmed by: the IR, mass spectroscopy, ^{1}H and ^{13}C NMR spectra, and were in satisfactory agreement with values found in the literature [40,41].

Ligand 4,4′-Dipyridylmonosulfide

Yield: 1805.4 mg (9.60 mmol, 64.0%). ^{1}H NMR (500.5 MHz, D_2O) δ/ppm: ^{1}H: 8.53 (d, 4H; H1, H5); 7.22 (d, 4H; H2, H4)). ^{13}C NMR (75.5 MHz, D_2O): δ/ppm: 149.12 (C1, C5), 145.44 (C3), 125.45 (C2, C4). IR (KBr, 4000–300 cm^{-1}): 3054 (m, N–H stretch); 1567, 1225 (C=N/C=C, pyridine ring stretch); 1107, 991 (C–H, aromatic stretch). TOF MS/ES^{+}. (*m/z*, MH^{+}): 189.05 ($C_{10}H_9N_2S$, species).

Synthesis of Pt(II) Complexes

The dinuclear platinum(II) complexes (**Pt1** to **Pt3**), [{*cis*-PtCl$(NH_3)_2$}$_2$-μ-dps]$(ClO_4)_2$ (**Pt1**), [{*cis*-PtCl$(NH_3)_2$}$_2$-μ-dpss]$(ClO_4)_2$ (**Pt2**), and [{*cis*-PtCl$(NH_3)_2$}$_2$-μ-bpe]$(ClO_4)_2$ (**Pt3**), were prepared by a reported procedure [41,42], starting from the precursor [{*cis*-PtCl$(NH_3)_2$(DMF)]ClO_4, using $AgClO_4$. Microanalytical data of the complexes are as follows.

Metal Complex Pt1. Yield: 62.8 mg (0. 069 mmol, 57.8%). ^{1}H NMR (500.5 MHz, D_2O) δ/ppm: ^{1}H: 8.78 (d, 4H); 7.60 (d, 4H). ^{195}Pt NMR (107.5 MHz, D_2O): δ/ppm: −2303.88. IR (KBr, 4000–300 cm^{-1}): 3179 (m, N–H stretch); 1598, 1480 (C=N/C=C, pyridine ring stretch); 1090–1100 (perchlorate counterion); 505 (Pt–N stretch); 302 (Pt–Cl stretch). TOF MS/ES^{+}. (*m/z*, M^{2+}): 358.005 ($C_{10}H_{18}N_6SPt_2Cl_2$ species). Anal. Calcd for $C_{10}H_{20}N_6SCl_4O_8Pt_2$: H, 2.20; C, 13.1; N, 9.17; S, 3.49. Found: H, 2.23; C, 13.45; N, 9.50; S, 3.35.

Metal Complex Pt2. Yield: 91.6 mg (0.097 mmol, 79.2%). ^{1}H NMR (500.5 MHz, D_2O), δ/ppm: 8.53 (d, 4H in dpss); 7.60 (d, 4H in dpss). ^{195}Pt NMR (107.5 MHz, D_2O) δ/ppm: −2304.16. IR (KBr, 4000–300 cm^{-1}): 3179 (N–H stretch); 1598, 1480 (C=N/C=C, pyridine ring stretch), 1421 (s, dpss), 1213 (w, dpss), 818 (m, dpss), 731 (m, dpss); 1090–1100 (perchlorate counterion); 507 (Pt–N stretch); 385 (Pt–Cl stretch). Anal. Calcd for $C_{10}H_{20}N_6Cl_4S_2O_8Pt_2$: H, 2.13; C, 12.65; N, 8.86; S, 6.76. Found*:* H, 2.19; C, 13.15; N, 8.82; S, 6.77.

Metal Complex Pt3. Yield: 52.5 mg (0. 058 mmol, 65.0%). ^{1}H NMR (500.5 MHz, D_2O) δ/ppm: 8.96 (d, 4H of py in bpe); 7.78 (d, 4H of py in bpe); 3.66 (s, 4H for $2CH_2$ of bpe). ^{195}Pt NMR (107.5 MHz, D_2O) δ/ppm: −2284.66. IR (KBr, 400–300 cm^{-1}): 3285 (N–H stretch); 1621 (C=N/C=C, pyridine ring stretch), 1436 (m, bpe), 1340 (vw, bpe), 1212 (w, bpe); 1090–1100 (perchlorate counterion); 556 (Pt–N stretch). TOF MS/ES^{+}. (*m/z*, M^{2+}): 356.535 ($C_{12}H_{22}N_6Pt_2Cl_2$, species). Anal. Calcd for $C_{12}H_{24}N_6Cl_4O_8Pt_2$: H, 2.65; C, 27.64; N, 9.21. Found: H, 2.59; C, 27.69; N, 9.71.

Preparation of the Dinuclear Pt(II) Diaqua Complexes

The chlorocomplexes (**Pt1, Pt2**, and **Pt3**) were converted into aqua analogues using the literature procedure [43]. The resultant aqua solutions were brought to a final complex concentration of 4.41 × 10^{-4}, 4.43 × 10^{-4}, and 1.13 × 10^{-4} M for [{*cis*-PtOH$_2$$(NH_3)_2$}$_2$-$\mu$-dps]$(ClO_4)_2$ (**Pt1**), [{*cis*-PtOH$_2$$(NH_3)_2$}$_2$-$\mu$-dpds]$(ClO_4)_2$ (**Pt2**), [{*cis*-PtOH$_2$$(NH_3)_2$}$_2$-$\mu$-bpe]$(ClO_4)_2$ (**Pt3**), respectively. The solution was acidified with $HClO_4$ to pH 1.0 (for the determination of pK_a values) and pH 2.0 (for kinetic measurements). The ionic strength was adjusted to 0.10 M with $NaClO_4$. The substitution reactions were studied in 0.10 M $NaClO_4$ at pH ca. 2.0, since the perchlorate ions do not coordinate with Pt(II) and to prevent deprotonation of the aqua ligand [20b, 44].

All kinetic experiments were performed under pseudo–first-order conditions, for which the concentration of the nucleophile was at least 20-fold in excess of appropriate metal complex to drive the reaction to completion. The substitution reactions of the complexes **Pt1**, **Pt2**, and **Pt3** with ligands thiourea (TU, DMTU, TMTU) and SCN^{-}, I^{-}, and Br^{-} were followed spectrophotometrically by monitoring the change in absorbance at suitable wavelengths as a function of time. The working wavelengths were determined by recording the spectra of the reaction mixture over the wavelength range 200–600 nm. These are recorded in Table S1 in the Supporting Information.

Spectrophotometric pK_a Titrations

The pH of the aqueous solutions was measured using a Jenway 4330 conductivity/pH meter equipped with a Micro 4.5 diameter glass electrode after calibration with standard buffers at pH 4.0, 7.0, and 10.0 at 25°C. The pH electrode was filled with 3 M NaCl

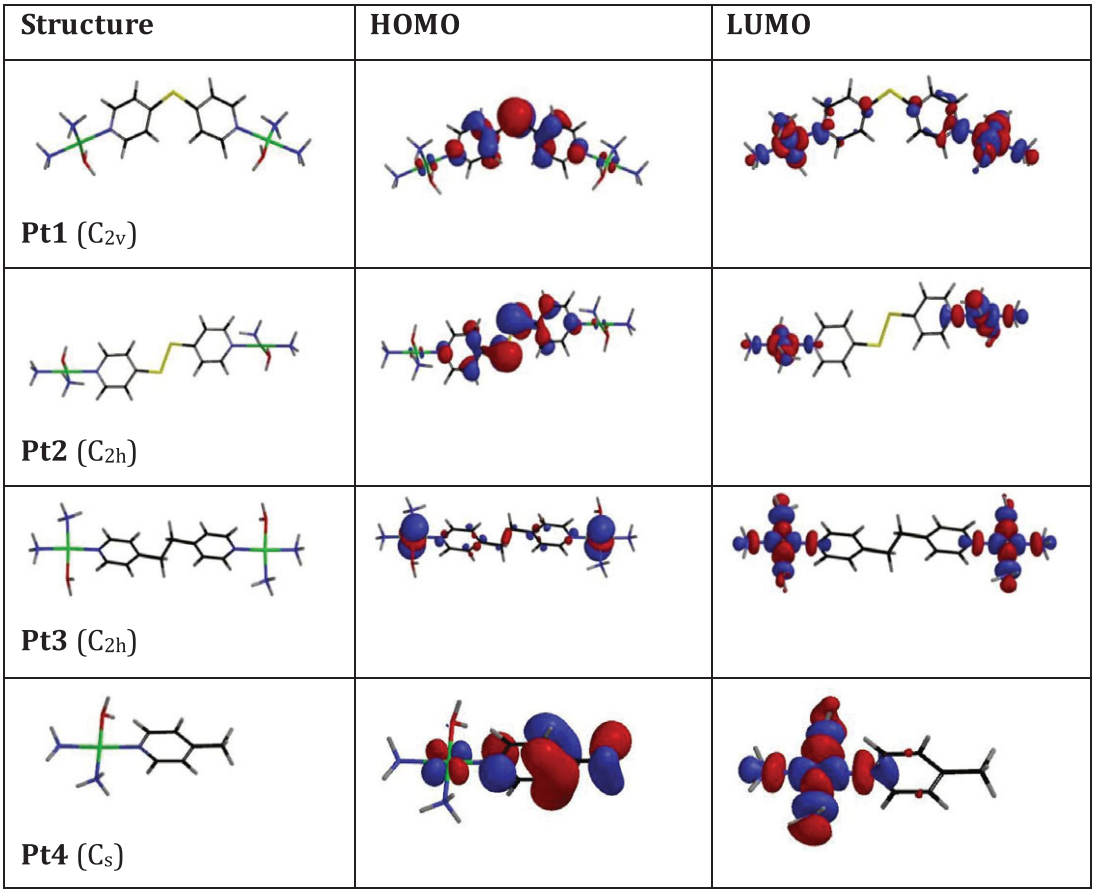

Figure 1 DFT optimized structures of the dinuclear platinum(II) complexes.

electrolyte to prevent precipitation of $KClO_4$ during use. A large volume (200 mL) of each of the complex solutions was used during the titrations to avoid absorbance corrections due to dilution, whereas spectrophotometric pH titrations were carried out using NaOH as the base. Subsequent pH changes were obtained by stepwise additions of crushed solid NaOH pellets in the pH range 2–3, micropipette dropwise addition of saturated, 1.0 and 0.1 M NaOH or concentrated $HClO_4$ (for reversibility of the pH) to the bulk of the complex solution, prior to withdrawal of 2 mL aliquots of the solution. After each of the measurements, the aliquots were not returned to the sample solutions to avoid in situ contamination by chloride ions from the pH electrode.

Quantum Chemical Computations

To gain insight into the connection between the structure and reactivity of the corresponding aqua complexes, as cations of total charges of +4, were optimized (in the gas phase) at the B3LYP [45] /LACVP** (Los Alamos Core Valence Potentials) [46] level. The Spartan® '04 for Windows® program was used. B3LYP relates to Becke's three parameter hybrid functional [45] that has been proven to be superior to traditional functionals. Figure 1 shows the minimum energy structures of the studied diaqua complexes calculated at the DFT (B3LYP/LACVP**) level of theory. Selected geometrical data including HOMO–LUMO, energy gap are summarized in Table I. The mononuclear complex, *cis*-$[Pt(H_2O)(NH_3)_2(4\text{-methylpyridine})]^{2+}$, **Pt4**, is included for comparative purposes with respect to the pK_a and DFT results of **Pt3**.

RESULTS AND DISCUSSION

Synthesis and Characterization of Compounds Pt1, Pt2, and Pt3

In this study, each of the three dinuclear Pt(II) complexes was prepared "in situ" from the cation *cis*-$[Pt(NH_3)_2(DMF)Cl]^+$. The DMF was selectively displaced by the ligands giving the desired dimer. The

Table I DFT-Calculated Parameters for the Dinuclear Platinum(II) Complexes

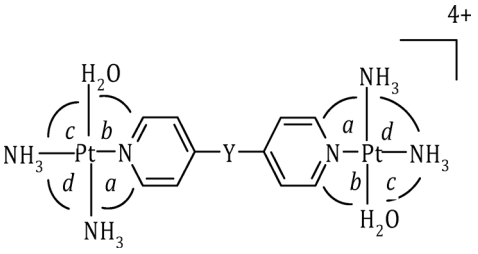

	Pt1	Pt2	Pt3	Pt4
HOMO–LUMO energy	S	S–S	C–C	C
HOMO (eV)	− 16.83	− 15.99	− 17.54	− 14.51
LUMO (eV)	− 12.62	− 12.21	− 12.21	− 9.59
(ΔE) (eV)	4.21	3.78	5.33	4.92
NBO charges				
Pt1/Pt2	1.207	1.206	1.205	1.199
Pt-OH/Pt-HO_2	1.177/1.201	1.173/1.201	1.169/1.201	
N_{py}	− 0.650	− 0.657	− 0.648	− 0.658
Bond length (Å)				
Pt-N_{py}	2.089	2.082	2.082	2.055
Pt-H_2O	2.128	2.129	2.128	2.126
Pt—Pt	12.07	13.74	13.54	
H_2O-Pt-NH_3 *cis to O*	2.484	2.493	2.475	
Ortho-H_{py}—Pt	3.006	3.013	3.027	
Bond angle (°)				
N_{py}-Pt- NH_3 trans to py	177.9	177.1	176.9	177.3
H_2O-Pt-NH_3 trans to O	175.6	176.1	176.1	178.9
b	94.4	93.4	93.4	93.3
a	90.0	90.3	90.5	87.9
c	83.7	83.7	83.5	84.1
d	92.4	92.5	92.6	94.8
Dipole moment (D)	1.93	4.01	0.16	2.18

details of the spectroscopic data for the ligand dps and the complexes are listed in the Experimental section. The characteristic IR bands at ca. 1570 cm^{-1} for the highest energy pyridine ring vibration of the ligands are shifted by ca. 25–29 to higher frequencies upon complexation, suggesting that the nitrogen atoms of pyridine are coordinated to platinum metal [47]. The presence of bands in the IR spectra of the perchlorate complexes at 1090–1100 cm^{-1} (O–Cl vibration stretch) indicates that ionic perchlorate is present as a counterion [44b]. In the ^{1}H NMR spectra of the three complexes, there are only two signals in the aromatic region, indicating that the structures of these complexes are symmetric due to coordination of the pyridyl rings at the Pt(II) centers. The ^{195}Pt signals for the three complexes appear within the range of −2284 to −2305 ppm, which is typical of (PtN_3) coordination environment [47].

Acidity of the Coordinated Aqua Ligands

To investigate the impact of the different diamine spacer groups on the reactivity of the diaqua Pt(II) complexes, the pK_a values of the coordinated water ligands were initially determined. A typical example of the UV–vis spectral changes observed during the pH titration with NaOH is shown in Fig. 2 for the **Pt3** complex and Fig. S1 in the Supporting Information. When the UV–vis data were fitted using a nonlinear least-squares procedure, as represented by the inset in Fig. 2, the pK_a values for the deprotonation of the coordinated aqua molecules were obtained from the standard Boltzmann equation.

The data gave an excellent fit for a system with two dissociation steps with equilibrium constants K_{a1} and K_{a2}, for which the overall process can be presented by the reaction given in Scheme 2.

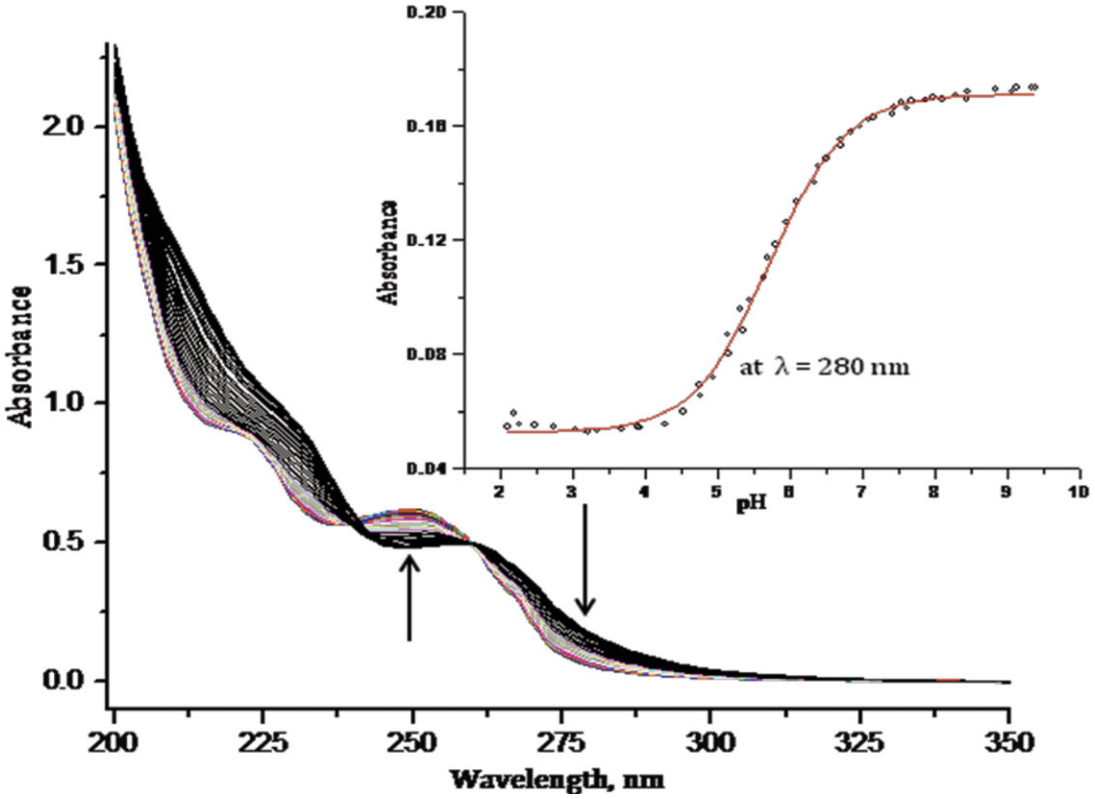

Figure 2 UV–vis spectra recored for 0.113 mM **Pt3** in the pH range 2–9 at 25°C ($I = 1.0$ M $NaClO_4$). Inset: Plot of absorbance versus pH at 280 nm for the **Pt3** complex.

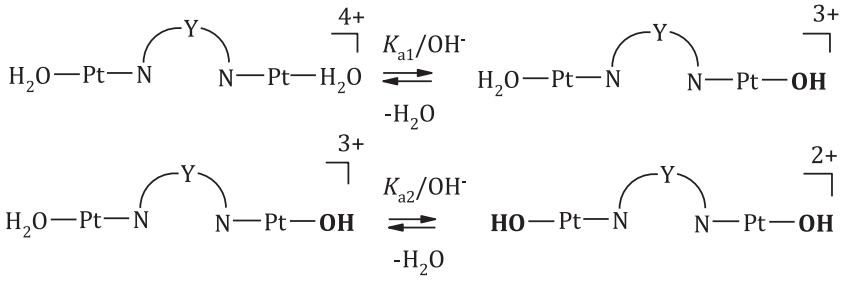

Scheme 2 Summary of the stepwise deprotonation of the dinuclear Pt(II) complexes as a function of pH.

Table II Summary of the pK_a Values Obtained for the Deprotonation of Platinum-Bound Water of the Different Complexes

Complex	**Pt1**	**Pt2**	**Pt3**	**Pt4**[a]
pK_{a1}	4.86 ± 0.05	5.19 ± 0.02	5.04 ± 0.15	5.63 ± 0.01
pK_{a2}	5.53 ± 0.03	6.42 ± 0.04	5.45 ± 0.17	N/A

[a]The pK_a value **is** obtained from [21a].

The pK_a values obtained are summarized in Table II. Included for comparison purpose in Table II is the pK_a value of the mononuclear analogue, *cis*-$[Pt(NH_3)_2(H_2O)(4\text{-methylpyridine})]^{2+}$, **Pt4** [21a].

Kinetic Measurements

The substitution reactions of the complexes with thioureas (TU, DMTU, and TMTU) and ionic nucleophiles (Br^-, I^-, SCN^-) were carried out at pH

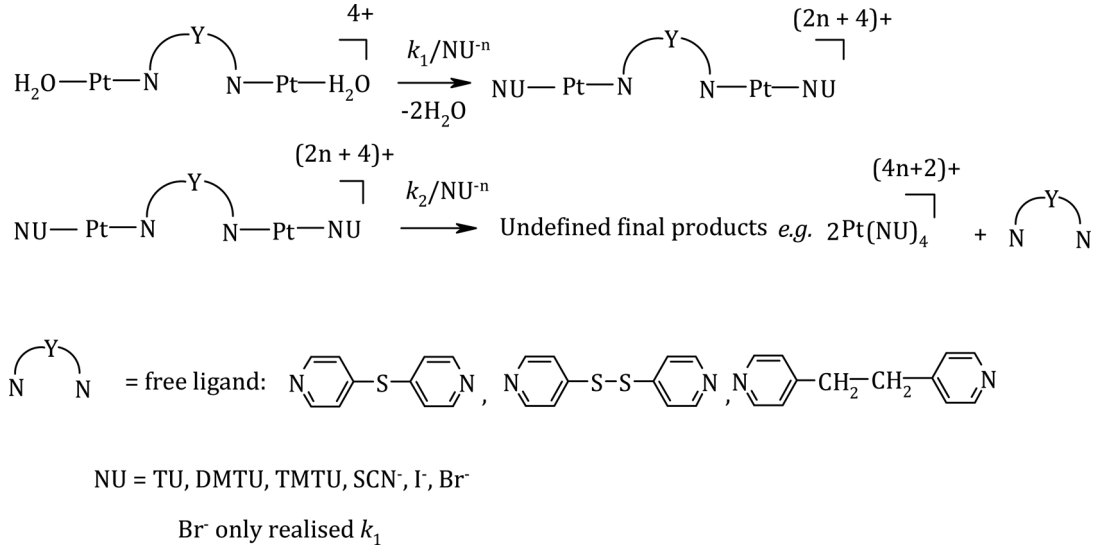

Scheme 3 Substitution mechanism for the reaction between the S, S–S, and C–C dinuclear Pt(II) complexes with selected nucleophiles.

Table III Kinetic Data for the Simultaneous Substitution of Aqua Ligands in $[\{cis\text{-}Pt(NH_3)_2H_2O\}_2L]^{4+}$ Complexes by Different Thiourea and Ionic Entering Nucleophiles; I = 0.10 M ($NaClO_4$), pH 2.0

Complex	NU	$k_{2,1st}$ (M^{-1} s^{-1})	$\Delta H^{\neq}_{1st}$ (kJ mol^{-1})	$\Delta S^{\neq}_{1st}$ (J mol^{-1} K^{-1})
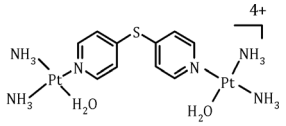 **Pt1**	TU	33.5 ± 0.5	63 ± 1.4	−41 ± 4.6
	DMTU	25.9 ± 1.1	56 ± 1.5	−64 ± 5.0
	TMTU	6.4 ± 0.1	58 ± 2.5	−57 ± 8.3
	SCN^-	14.0 ± 0.6	60 ± 4.9	−52 ± 16.3
	Br^-	0.4 ± 0.01	73 ± 2.3	−26 ± 7.5
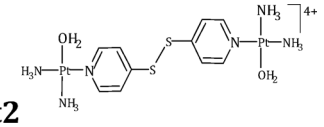 **Pt2**	TU	244.6 ± 2.9	53 ± 0.4	−52 ± 1.4
	DMTU	179.0 ± 2.8	48 ± 2.8	−111 ± 9.3
	TMTU	86.2 ± 1.8	48 ± 1.6	−91 ± 5.4
	SCN^-	542.0 ± 14.1	69 ± 1.0	−26 ± 3.4
	Br^-	13.0 ± 0.2	74 ± 2.3	−25 ± 7.7
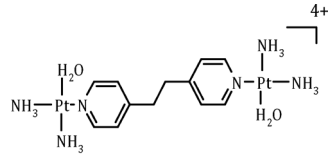 **Pt3**	TU	129.5 ± 1.6	53 ± 0.4	−53 ± 1.3
	DMTU	65.6 ± 0.6	44 ± 1.6	−85 ± 5.5
	TMTU	13.4 ± 0.2	41 ± 0.5	−112 ± 1.8
	SCN^-	258.2 ± 2.5	54 ± 3.0	−39 ± 10.0
	I^-	129.5 ± 1.6	42 ± 1.7	−83 ± 5.6
	Br^-	11.8 ± 0.2	50 ± 2.0	−104 ± 6.6

The standard deviations reported are from the least-squares fits to Eq. (1). At pH 2.0, the S–S bond scission occurred reversibly in a redox reaction with iodide: py–S–S-py + $2I^- \leftrightarrow 2py\text{–}S^- + I_2$. This limited further kinetic studies for **Pt1** and **Pt2** complexes.

2.0. The purpose of keeping the solutions acidic was to make sure that the complex remains in the aqueous form and at the same time protonate the released N-donor pyridyl bridging ligand so as to prevent any probability of its recoordination to the metal center, as shown in Scheme 3. Besides, protonation of thiourea (TU, $pK_a = -1.3$) can be ruled out as reported recently [48]. As already mentioned, all the kinetic measurements were done under pseudo–first-order conditions with respect to the nucleophile, to drive the reactions to completion.

Because of being a weak nucleophile, the results of the substitution reaction with bromide for all the studied complexes gave only one substitution process (Table III). However, the substitution reactions of the aqua complexes with nucleophiles of stronger nucleophilicity like the thioureas (TU, DMTU, and TMTU) and the other anionic nucleophiles (I^-, SCN^-) showed two reaction steps. The first step is attributed to simultaneous substitution of both aqua ligands by the nucleophiles. The second step is much slower by one to three orders of magnitude compared to the first step

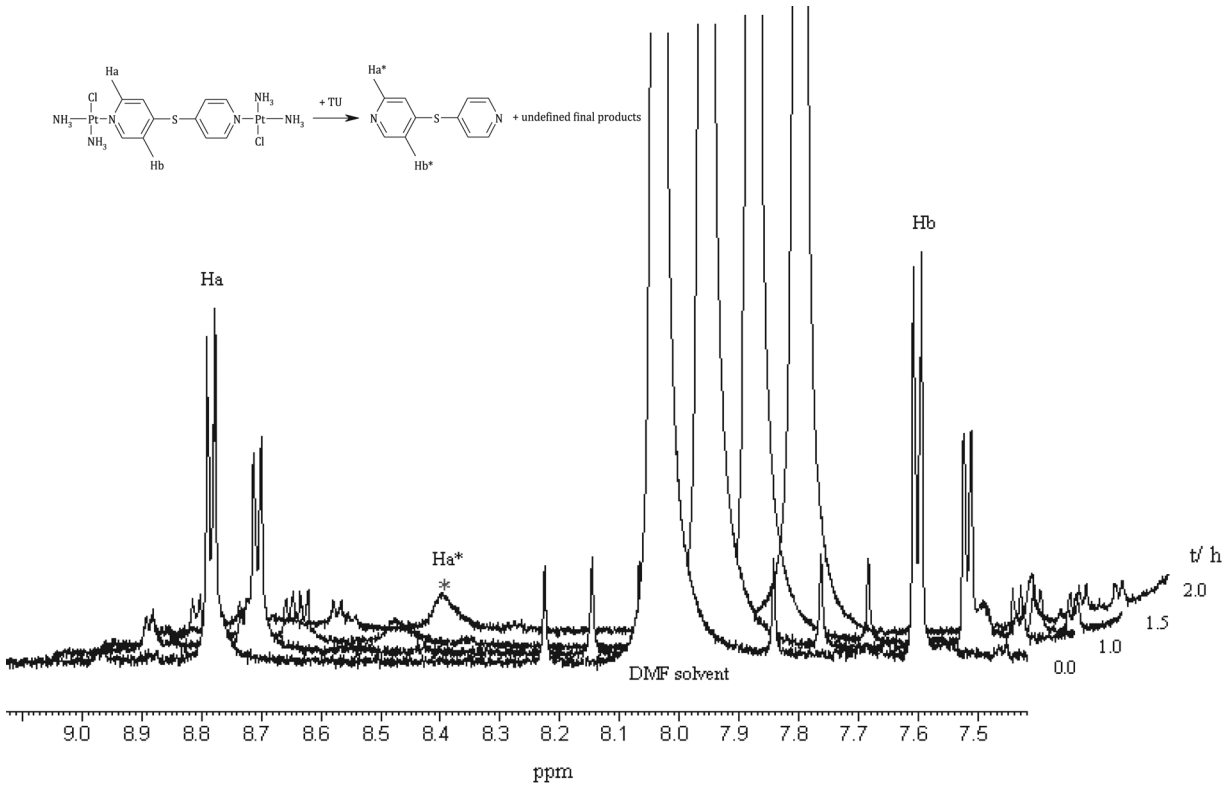

Figure 3 The ^{1}H NMR spectra of the reaction of **Pt1–Cl** with thiourea (2.0 mM) in DMF-d_7, at 30°C showing the release of the 4,4′-bis(pyridine)sulfide bridging ligand.

and is assigned to the release of the linker following coordination of further nucleophiles to the Pt(II) center. Evidence for the bridging ligands release comes by monitoring the reaction between **Pt1-Cl** and TU (6 equiv.) by ^{1}H NMR spectroscopy in DMF-d_7. An array of the proton NMR spectra, showing the aromatic region only, is recorded in Fig. 3. The adopted numbering system for the pyridyl protons Ha/Hb used to monitor the progress of the reaction is shown on the structure of the **Pt1–Cl** complex as an inset in Fig. 3. The signals of the coordinated bridging ligand appear at $H_a = 8.78$ and $H_b = 7.60$ ppm as doublet resonances, which decreased during the reaction. After 1.5 h of the reaction, a broad singlet signal was observed at $H_a^* = 8.53$ ppm, representing the released (free) 4,4′-bis(pyridine)sulfide bridging ligand. This agrees with the values reported in the literature [40]. However, the H_b^* signal at 7.22 ppm expected for the second aromatic proton of freed ligand was obscured by the broad peak due to thiourea (TU) at 7.20 ppm and is not shown on Fig. 3. Since the excess thiourea displaces the last N-donor atoms in the bridging system releasing the linker, undefined final products such as $[Pt(TU)_4]^{2+}$ are also liberated as has been reported by our group [30].

Because of the low concentration of the **Pt1–Cl** complex, the aromatic resonances corresponding to the unreacted complex appear as downfield–shifted peaks as the reaction progressed. This is consistent with what has been reported before for bidentate-coordinated Pt(II)-based species like DNA intercalators [49].

It can be concluded that substitution of the aqua ligands at each of Pt(II) centers occurs simultaneously in all the complexes investigated irrespective of the nature of the spacer group. This is consistent with the symmetrical nature of the complexes. But the second and slower subsequent step is due to the strong labilizing thiourea and other nucleophiles inducing dissociation of the linker. The second step is also sensitive to variations in the nature and size of the spacer group of the pyridyl moiety. Thus, the overall substitution process can be represented by the reactions shown in Scheme 3.

In all cases, the first step was fast and was therefore studied on the stopped-flow reaction analyzer, whereas the subsequent slower step was studied by the UV–vis spectroscopic method. The general course of the substitution reactions for 1.0 mM **Pt2** with 3.0 mM TU is recorded in Fig. 4.

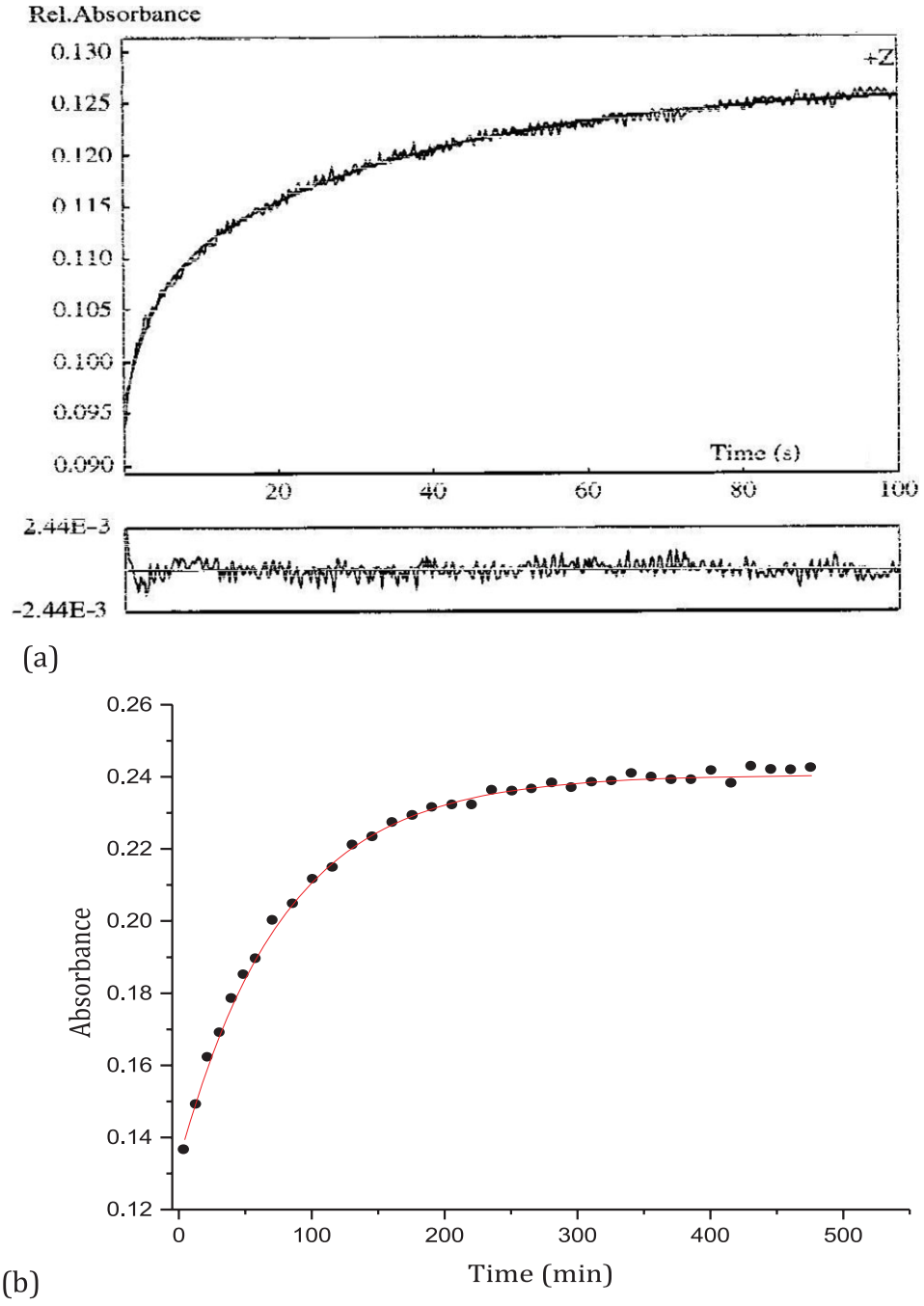

Figure 4 Absorbance–time traces for the reaction between **Pt2** (1.13×10^{-1} mM) and TU (1.03 mM) on (a) a short time scale for $k_{2(1st)}$ on stopped flow and (b) a long time scale for $k_{2(2nd)}$ by the UV–vis spectrophotometric method at 305 nm, $T =$ 298 K, $I = 0.10$ M (0.01 M $HClO_4$, adjusted with $NaClO_4$), pH 2.0.

Both the first and second substitution steps fitted well to a single-exponential model to give the observed rate constants $k_{obs(1st)}$ and $k_{obs(2nd)}$. The observed pseudo–first-order rate constants, $k_{obs(1st/2nd)}$, were calculated as the average value from four to six independent kinetic runs using the Origin 7.5® program. The determined pseudo–first-order rate constants, $k_{obs(1st/2nd)}$, were plotted against the nucleophile concentration. A linear dependency of the observed rate constants on the concentration of the nucleophiles was obtained as shown for the **Pt1** complex in Figs. 5 and 6 (also Figures S2–S5 for **Pt3** and **Pt2** in the Supporting Information). The second-order rate constants, $k_{2(1st/2nd)}$, were derived from the slopes of the

Table IV Kinetic Data for the Release of the Linker in $|\{cis\text{-}Pt(NH_3)_2H_2O\}_2L|^{4+}$ Complexes by Different Thiourea and Ionic Entering Nucleophiles; I = 0.10 M ($NaClO_4$), pH 2.0

Complex	NU	$k_{2,2nd}$ (10^{-3} M^{-1} s^{-1})	$\Delta H^{\neq}_{2nd}$ (kJ $mol^{-1)}$	$\Delta S^{\neq}_{2nd}$ /J (mol^{-1} K^{-1})
Pt1	TU	102.1 ± 0.20	49 ± 3.2	−107 ± 10.7
	DMTU	51.5 ± 0.64	53 ± 0.6	−99 ± 1.9
	TMTU	70.6 ± 1.52	48 ± 1.9	−117 ± 6.4
	SCN^-	39.0 ± 0.28	65 ± 1.7	−61 ± 5.8
Pt2	TU	35.4 ± 0.23	53 ± 1.3	−95 ± 4.5
	DMTU	14.3 ± 0.05	62 ± 1.1	−73 ± 3.6
	TMTU	24.9 ± 0.12	49 ± 0.9	−116 ± 2.9
	SCN^-	18.8 ± 0.41	49 ± 1.0	−83 ± 3.5
Pt3	TU	23.8 ± 0.18	59 ± 1.2	−80 ± 4.1
	DMTU	7.6 ± 0.36	49 ± 1.2	−122 ± 4.1
	TMTU	1.4 ± 0.22	50 ± 1.1	−133 ± 3.6
	SCN^-	14.7 ± 0.14	49 ± 1.1	−78 ± 3.5
	I^-	1.2 ± 0.14	50 ± 1.2	−133 ± 3.9

The standard deviations reported are from the least-squares fits to Eq. (1). Br^- = No reaction was observed in the complexes.

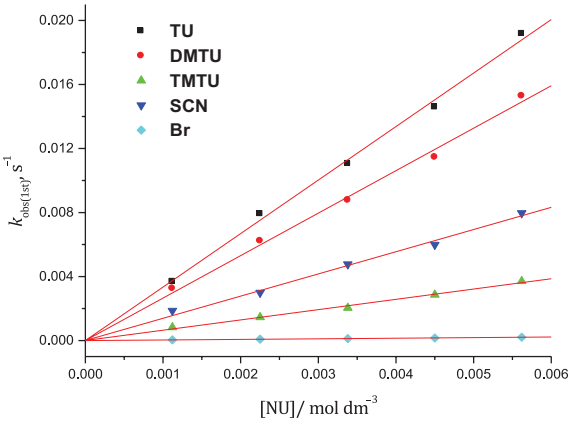

Figure 5 Plot of $k_{obs(1st)}$ versus thiourea and the ionic nucleophile concentration for the simultaneous substitution of aqua ligands in **Pt1** at pH 2.0, T = 298.15 K, I = 0.10 M (0.01 M $HClO_4$, adjusted with $NaClO_4$).

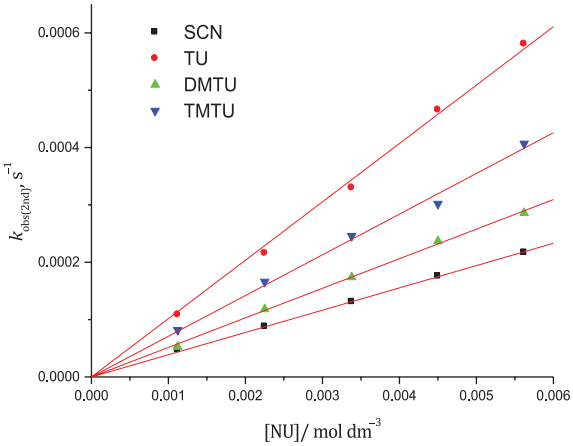

Figure 6 Plot of $k_{obs(2nd)}$ versus thiourea and the ionic nucleophile concentration for the dissociation of the bridging ligand in **Pt1** at pH 2.0, T = 298.15 K, I = 0.10 M (0.01 M $HClO_4$, adjusted with $NaClO_4$).

plots and are summarized for all the complexes investigated in this study in Tables III and IV.

None of the plots exhibited a nonzero intercept in all the reactions of the complexes with the nucleophiles, indicating that both steps are irreversible in nature, and k_{-1} and k_{-2} representing reversible reactions are zero since the reverse reaction is too slow, if it exists. Thus, the rate equations for the two substitution reaction steps can be expressed by Eq. (1):

$$k_{obs(1st/2nd)} = k_{2(1st/2nd)}[NU] \quad (1)$$

Activation Parameters

To confirm that these complexes follow an associative substitution mode characteristic of square-planar complexes, the reactions were studied at different temperatures in the range 15–35°C, at 5°C interval. The Eyring plots recorded in Figs. 7 and 8 (also Figures S6–S9 for **Pt3** and **Pt2** in the Supporting Information) resulted in the following activation parameters: activation enthalpy, $\Delta H^{\neq}_{(1st/2nd)}$ from the slopes and activation entropy, $\Delta S^{\neq}_{(1st/2nd)}$ from the intercept. The activation entropies in Tables III and IV for all the reactions studied suggest increased order in the transition state, indicative of an associative mode of the substitution mechanism.

DFT Calculations

The geometry about the Pt atoms is slightly distorted square planar as observed from the bond angles

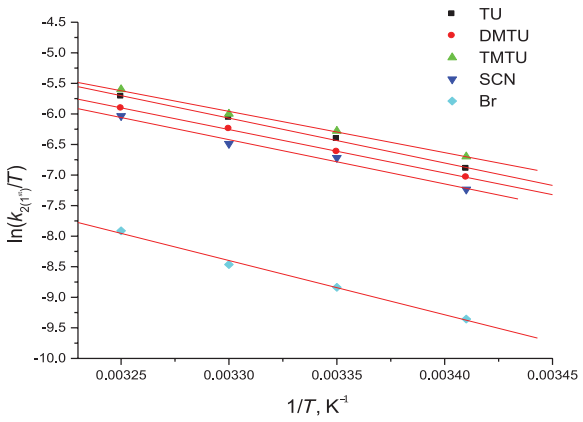

Figure 7 Plots of $\ln(k_{2(1st)}/T)$ versus $(1/T)$ for the simultaneous substitution of aqua ligands in **Pt1** with a series of different nucleophiles at pH 2.0, $T = 298.15$ K, $I = 0.10$ M (0.01 M $HClO_4$, adjusted with $NaClO_4$).

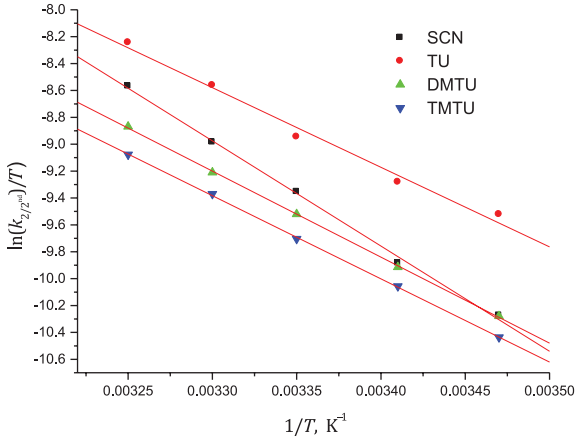

Figure 8 Plots of $\ln(k_{2(2nd)}/T)$ versus $(1/T)$ for the release of the bridging ligand in **Pt1** with a series of different nucleophiles pH 2.0, $T = 298.15$ K, $I = 0.10$ M (0.01 M $HClO_4$, adjusted with $NaClO_4$).

presented in Table I. It is also noted that the angle labeled *C* is smaller than all the other angles around the Pt(II) center, indicating possibility of the hydrogen-bonding interaction between the H_2O/NH_3 moieties (average separation distance = 2.484 Å). The NBO charges on the platinum atoms (Table I), to a large extent, remain almost constant across the series of the investigated complexes. This is not unexpected, since X-ray structures of other Pt(II) complexes with such aromatic bridging ligands (e.g., 4,4′-bis(pyridine)ethane, 4,4′-bis(pyridine)sulfide, 4,4′-bis(pyridine)disulfide) indicate that the aromatic ring lies almost perpendicular to the plane of the Pt(II) center [23,50]. Therefore, the interaction between the metal center and the pyridine ring through π-backbonding is expected to be extremely small, if it exists.

The DFT calculations also reveal that the major influence of the para-substituent (Y), i.e., *pyridyl 4-position*, is on the HOMO energy level "ground-state effect" and not the LUMO (Fig. 1). The electron density of the HOMO orbitals is localized between the pyridyl π-acceptor bridging ligand and the spacer S atom(s) in **Pt1** and **Pt2**, whereas in **Pt3** the HOMO orbitals lie entirely on the Pt(II) centers and very sparsely on the bridging moiety. In the case of the LUMO orbitals, these consist of contributions from the metal centers and the donor atoms of the am(m)ine ligands in all the three complexes. The effect of increasing the number of S-atoms results in decreasing the HOMO–LUMO energy gap, whereas replacing the S atoms with the $–CH_2–CH_2–$ group raises the energy level as the data in Table I show.

From this study, the most important structural features revealed by the optimized structures shown in Fig. 1 and the data in Table I are that the structural geometry of each complex depends on the angular conformation of the spacer group. For instance, when the sp^3 hybridized S atom is incorporated between the two pyridine rings in the **Pt1** complex, it assumes a V-shaped structure, which results in a C_{2v} point group symmetry. In the case of **Pt2** and **Pt3**, the pyridyl units run nearly parallel, which adopts a slip-up structure that belongs to the C_{2h} point group symmetry. Such a structure resembles that of dinuclear Pt(II) complexes bridged by the flexible α,ω-alkyldiamine, with $(CH_2)_n$ groups that have even numbers of carbon atoms [24, 25b].

The conformational differences significantly influenced the DFT calculated values of the Pt—Pt separation distances (through space), i.e., **Pt1** (12.07), **Pt2** (13.74), and **Pt3** (13.54 Å), and the dipole moments exhibited by **Pt1** (1.93), **Pt2** (4.01), and **Pt3** (0.16 D) recorded in Table I. These structural metrics are brought about by the smaller C–C (Å) bond length relative to that of S–S (Å) due to the larger covalent radius of the S atom compared to carbon and also are influenced by the symmetry of the complex. These structural features together with the steric influences on the square-planar planes at the Pt(II) centers, as will be discussed later, are expected to control reactivity with the incoming nucleophiles.

pK_a Determination for the Diaqua Complexes

The thermodynamic data in Table II demonstrate that the pK_a values of the coordinated aqua moieties are dependent on the nature of the bridging ligand. The

pK_{a1} values of the studied dinuclear complexes **Pt1**, **Pt2**, and **Pt3** (ranging from 4.86 ± 0.05 to 5.19 ± 0.02) are lower than those of the mononuclear analogues **Pt4** ($pK_a = 5.63 \pm 0.01$) [21a] and the Pt(II) amphiphiles recently published [51]: $[Pt(H_2O)(N,N\text{-bis(2-pyridylmethyl)-NCH}_2)_n\text{-CH}_3;\ NH]^{2+}$ $n = 1, 2, 3, 4, 5, 9$ ($pK_a = 5.45 \pm 0.05$ to 5.52 ± 0.02). This signifies an increase in acidities of the coordinated water molecules in the investigated dinuclear complexes in this study. This is in agreement with what has been reported in other studies, which have shown Pt atoms in dinuclear complexes to be more acidic than the Pt atoms of the mononuclear analogues [24, 25, 51]. A higher overall positive charge of 4^+ coupled with higher electrophilicity on the Pt atoms is the reason for the lower pK_a values observed in the dinuclear complexes than that found for 2+ charged Pt(II) centers of the mononuclear complexes. Furthermore, a short distance between the Pt(II) center of the dinuclear complexes, results in single charge additions (controlled by in-space electrostatic forces and/or H bond) on the platinum atoms that increases the effective positive charge at the metal center [25b,c]. This explains why with decreasing Pt—Pt separation distance the pK_{a1} values become smaller.

Moreover, since the position of the ^{195}Pt resonance is influenced by the donor strength of the ligands attached to the platinum metal center [52], the results indicate that the σ-inductive effect of para-substituent on the pyridyl linker toward the Pt(II) center differ in strength and as a result influences the bacisity of the aqua complexes. This is supported by the differences in the ^{195}Pt NMR chemical shifts of **Pt1** (−2303.9), **Pt2** (−2304.2), **Pt3** (−2284.7), and **Pt4** (−2299 ppm), respectively. However, from Table I, the DFT calculated NBO charges are statistically constant, indicating that the influence of the σ-donor properties of the pyridyl-bridging moiety on the positive charge on the metal center is insignificant and hence plays little or no important role on the p*K*a values and also on the electrophilicity of the Pt atoms of the complexes. In addition, the difference of only 0.3 pK_{a1} units between pK_{a1} values of the complexes of shortest and longest spacer length shows the result is more of a charge–addition effect than the σ–donor effect by the bridging ligand. The pK_{a1} value of the diaqua **Pt3** complex is in agreement with the recently published value for its trans-isomer [35c].

Further observation shows that deprotonation of the second coordinated water molecule to the hydroxo/hydroxo species occurs at higher pH values than in the first step in all the three complexes. This is due to a reduction of the overall charge to +3 after deprotonation of one coordinated water molecule. The Pt(II) center of the aqua/hydroxo species is thus less electrophilic and less acidic compared to that of the parent diaqua complex [25,32], leading to higher pK_{a2} values. As already mentioned for the first deprotonation step, the pK_{a2} values also depend on the nature and length of the spacer group.

These σ–inductive effects on the ground-state properties of the Pt(II) complexes are also supported by the computational data. The DFT calculated NBO charges at the Pt(II) centers decreased after deprotonation of the first water molecule compared with values of the diaqua complexes (Table I). The trend for the second pK_as is also in the order of the magnitude of the dipole moments of the complexes, which is a measure of the electronegativiy of the complexes.

Kinetic Analysis

Based on the DFT calculated Pt—Pt distances of the complexes and the small change in NBO charge after the deprotonation of the first coordinated water molecule, one can conclude that the distances are long enough to prevent strong intramolecular "electronic communication" between the two Pt(II) centers. This makes the two Pt(II) centers kinetically indistinguishable from each other, and therefore, react independently. Analysis of the rate constants (Table III) shows that the two metal centers could not be discriminated by the incoming nucleophiles, resulting in the simultaneous substitution of both labile aqua ligands as the first reaction step.

From the values of the second-order rate constants for the direct attack pathway, k_1 (Table III), the order of reactivity of the diaqua Pt(II) complexes, is **Pt2** > **Pt3** > **Pt1**. The difference in reactivity can be attributed to steric and electronic effects attributed to different structural or geometrical arrangement of the spacer atom(s) of the pyridyl linker.

It is widely accepted that the pK_a value of the coordinated water molecule is an indicator of the electron density around the metal center and hence, of the electrophilicity of the Pt(II) center [19,50]. Since the pK_{a1} value of the **Pt1** complex is smaller than that of either **Pt2** or **Pt3**, one would expect higher reactivity for **Pt1**. The data in Table III show the contrary. In addition, enhanced reactivity due to the "entrapment effect" expected of complexes with the C_{2v} point group symmetry [24], was also not observed in the first substitution step of **Pt1**. As seen from the optimized structure of the complex (Fig. 9), the central cavity is blocked by the pyridine ring that protrudes into the cavity preventing the entrapment effect to the nucleophiles. The DFT calculated C–S–C angles of 94.5 and 112.8° for the 4,4′-bis(pyridine)sulfide ligand and the **Pt1**

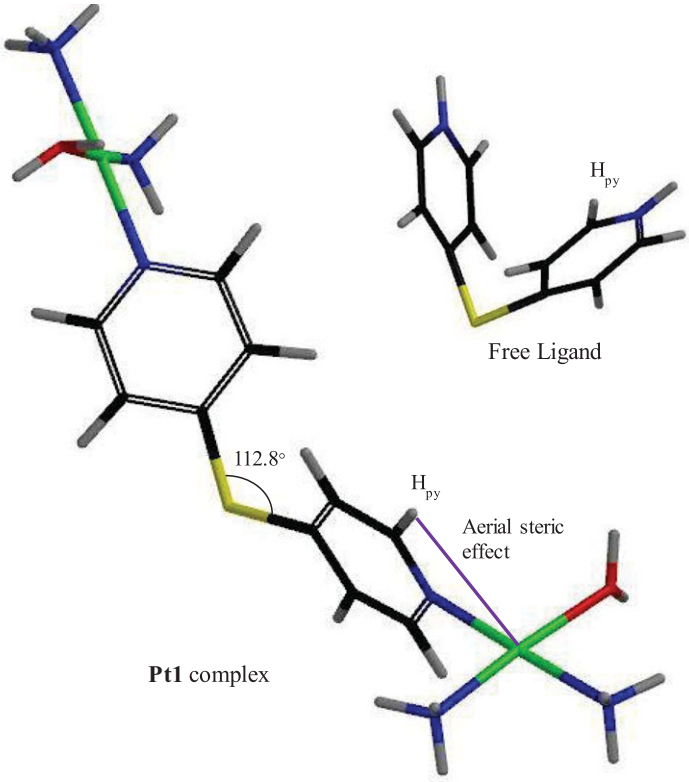

Figure 9 Schematic structures of **Pt1** and free ligand illustrating the twisted conformation and steric factor of **Pt1**.

complex, respectively, show that the ligand has a perfect V-shaped planar structure (C_{2v}), whereas **Pt1** is highly distorted (Fig. 9). The lone pairs on the sp^3 hybridized S atom in **Pt1** occupy less geometrical angles about the atom and cause greater repulsions, which forces the Pt coordination planes to sit in a twisted anticonformation relative to each other as seen in Fig. 9. The pyridine ring is inclined at an angle that is almost perpendicular to the Pt(II) center, such that the *ortho*-hydrogen atom on the aromatic ring (H_{py}) poses steric influence to aerial approach of the entering ligand on each Pt(II) center, leading to a slower nucleophilic attack. It can be presumed that an equal amount of steric influence is felt by the Pt atoms of the investigated dinuclear complexes. However, the DFT-calculated inclination distance between the *ortho*-hydrogen atom and the Pt(II) center (H_{py}—Pt) increases in the order 3.006, 3.013, and 3.027 Å (Table I) for **Pt1**, **Pt2**, and **Pt3**, respectively, showing that the greatest steric hindrance is present in **Pt1**. The observed distortion of the bridging ligand in **Pt1** is absent in **Pt2**.

To understand further the role of the linker on the rate of substitution, the reactivity of **Pt2** and **Pt3** is compared. **Pt2** and **Pt3** complexes both adopt C_{2h} molecular point symmetry, but differ by what links together the two pyridines attached to the Pt atoms. This difference makes the **Pt2** complex to have the highest dipole moment (Table I), an indication that its Pt(II) cent$_{er}$ is more electrophilic, as such it could be more reactive in comparison to the other complexes as observed. This is supported by the NBO charge on **Pt3**, which is slightly less positive compared to that of **Pt2**. In addition, the HOMO–LUMO energy gap (Table I) is wider for **Pt3** than for **Pt2**, suggesting an increase in the energy barrier and therefore a slower substitution reaction.

A further observation is that the second step is remarkably slower than the simultaneous substitution of the aqua ligands in the first step in all cases. It is assigned to the release of the bridging pyridyl ligand following the coordination of further nucleophiles to the already sterically crowded Pt(II) center. The pyridine-bridging ligand can engage in "synergistic σ-/π-bonding" [53]. This type of bonding should be less dependent on the availability of σ-electrons but has the flux of electrons primarily from the metal center to the ligand via the electronegative N–atom on the ring. This enhances the electrophilicity of the Pt(II) center, allowing direct attack by the incoming nucleophiles. Because of these factors, the congested Pt(II) center in the transition state weakens the bonds, forcing the dissociation of pyridyl linker. The order of

reactivity of the complexes is **Pt1** > **Pt2** > **Pt3**, mostly controlled by the structural differences. The entrapment of the incoming nucleophiles coupled with the release of steric strain imposed on the structure by lone pair repulsions in the twisted conformation in **Pt1** accounts for its much higher reactivity compared to **Pt2** and **Pt3**.

The reactivity of the thiourea nucleophiles at the Pt(II) centers during the simultaneous substitution of the aqua ligands increases in order TU > DMTU > TMTU, which reflects the steric characteristics of a mechanism involving bond making in the five-coordinate transition state. The most sterically hindered nucleophile TMTU reacts significantly slower than the less hindered TU in all cases. The order of reactivity for the anionic nucleophiles is $SCN^- > I^- > Br^-$, which is in line with the polarizability of the ions, i.e., 3.05×10^{-24}, 4.70×10^{-24}, and 6.1×10^{-24} cm^3 for Br^-, I^-, and SCN^-, respectively [54,55], and electrostatic attraction forces between the anions and the doubly charged terminal Pt(II) centers [56].

The large negative activation entropies ($\Delta S^{\neq}_{(1st/2nd)}$) indicate that the substitution of the aqua ligands and the release of the linker from the Pt(II) metal center proceed via an associative substitution mechanism dominated by bond making in the transition state [57,58]. This actually is acceptable since the Pt(II) metal center is a soft classic 16 electron species that allows easier substitution of the aqua ligands and dissociation of the linker in the rate-determining step. This is confirmed by ^{1}H NMR spectroscopy.

CONCLUSIONS

In the present study, substitution reactions of three dinuclear Pt(II) complexes containing different pyridyl bridging ligands with selected entering nucleophiles were investigated. The obtained results show that the nature of the spacer group incorporated on the structure of the bridging ligand significantly influences the pK_a and substitution reactivity of the Pt(II) complexes. In all the complexes, the two Pt(II) centers are independent, so it was possible to determine two pK_a values. The pK_a values increased in the order **Pt1** < **Pt3** < **Pt2,** which can be attributed to decreasing charge additions and communication between the two Pt atoms as the separation distance increases. The substitution kinetics resulted into two substitution reaction steps, one being simultaneous substitution of the labile aqua ligands followed by the release of the bridging ligand. The order of reactivity is **Pt1** < **Pt3** < **Pt2** for the simultaneous substitution of the aqua ligands, whereas for the dissociation of the linker it is **Pt1** > **Pt2** > **Pt3**. The **Pt1** complex reacts slower than the other complexes due to nonplanarity of the 4,4′-dipyridinesulfide bridging ligand. Namely, the aerial steric hindrance associated with the ortho-proton (H_{py}) on the pyridine ligand significantly prevents the substitution, whereas the release of strain on the bridge increases dissociation of the bridging ligand in the second step. It can be concluded that the dissociation of the linker is a possible indication that if these compounds are used for treatment of cancer, they are likely to be unstable. The substitution process of the studied systems remains the associative mechanism supported by the negative entropies of activation.

The authors gratefully acknowledge financial support and Ph.D. bursary for P. O. Ongoma from the University of KwaZulu-Natal and the National Research Foundation (NRF, South Africa) and Egerton University, Kenya.

BIBLIOGRAPHY

1. Cummings, R. E.; J.; Ritchie, A. A.; Muir, M.; Morris, R. E.; Chen, H. Br J Cancer 2002, 86, 1652.
2. Lippard, S. J.; Wang, D. Nat Rev Drug 2005, 4, 307.
3. Miller, S. E.; House, D. A. Inorg Chim Acta 1990, 173, 53.
4. Momekov, G.; Bakalova, A.; Karaivanova, M. Curr Med Chem 2005, 12, 2177.
5. (a) Zhang, C. X.; Lippard, S. J. Curr Opin Chem Biol 2003, 7, 481; (b) Jung, Y.; Lippard, S. J. Chem Rev 2007, 107, 1387.
6. Pantoja, E.; Gallipoli, A.; Van Zutphen, S.; Komeda, S.; Reddy, D.; Jaganyi, D.; Lutz, M.; Tooke, M. D.; Spek, A. L.; Ravarro-Ranninger, C.; Reedijk, J. J Inorg Biochem 2006, 100, 1955, and references cited therein.
7. (a) Natile, G.; Coluccia, M. Coord Chem Rev 2001, 216, 383; (b) Dyson, P. J.; Sava, G. Dalton Trans 2006, 1929.
8. Hambley, T. W. Coord Chem Rev 1997, 166, 181.
9. Wheate, N. J.; Walker, S.; Craig, G. E.; Oun, R. Dalton Trans 2010, 39, 8113.
10. (a) Sykes, A. G. Platinum Met Rev 1988, 32, 170; (b) Pasini, A.; Zunino, F. Angew Chem, Int Ed 1987, 26, 615; (c) Farrell, N.; Qu, Y.; Hacker, M. P. J Med Chem 1990, 33, 2179.
11. Reedjik, J. Platinum Met Rev 2008, 52, 2.
12. Rubino, S.; Portanova, P.; Giammalva, F.; Girasolo, M. A.; Orecchio, S.; Calvaruso, G.; Stocco, G. C. Inorg Chim Acta 2011, 370, 207, and references cited therein.
13. (a) Kalinowska-Lis, U.; Ochocki, J.; Matlawska-Wasowska, K. Coord Chem Rev 2008, 252, 1328; (b) Wheate, N. J.; Collins, J. G. Coord Chem Rev 2003, 241, 133; (c) Jansen, B. A. J.; Van Der Zwan, J.; den Dulk, H.; Brouwer, J.; Reedijk, J. J Med Chem 2001, 44, 245.
14. Komeda, S.; Lutz, M.; Spek, A. L.; Chikuma, M.; Reedijk, J. Inorg Chem 2000, 39, 4230.

15. Komeda, S.; Kalayda, G. V.; Lutz, M.; Spek, A. L.; Yamanaka, Y.; Sato, T.; Chikuma, M.; Reedijk, J. J Med Chem 2003, 46, 1210.
16. Kalayda, G. V.; Komeda, S.; Ikeda, K.; Sato, T.; Chikuma, M.; Reedijk, J. Eur J Inorg Chem 2003, 4347.
17. Wendt, O. F.; Elding, L. I. J Chem Soc, Dalton Trans 1997, 4725.
18. Reddy, D.; Jaganyi, D. Dalton Trans 2008, 6724.
19. Hofmann, A.; Jaganyi, D.; Munro, O. Q.; Liehr, G.; van Eldik, R. Inorg Chem 2003, 42, 1688.
20. (a) Krüger, H.; van Eldik, R. J Chem Soc, Chem Commun 1990, 330; (b) Pitteri, B.; Bortoluzzi, M. Polyhedron 2008, 27, 2259.
21. (a) Jin, V. X.; Tan, S. I.; Ranford, J. D. Inorg Chim Acta 2005, 358, 677; (b) Wong, E.; Giandomenico, C. M. Chem Rev 1999, 99, 2451.
22. Sarmah, P.; Deka, R. C. J Mol Str: THEOCHEM 2010, 955, 53.
23. Reddy, D.; Jaganyi, D. Int J Chem Kinet 2011, 43, 161.
24. Mambanda, A.; Jaganyi, D.; Hochreuther, S.; van Eldik, R. Dalton Trans 2010, 39, 3595.
25. (a) Hofmann, A.; van Eldik, R. Dalton Trans 2003, 2979; (b) Ertürk, H.; Hofmann, A.; Puchta, R.; van Eldik, R. Dalton Trans 2007, 2295; (c) Ertürk, H.; Maigut, J.; Puchta, R.; van Eldik, R. Dalton Trans 2008, 2759.
26. Jaganyi, D.; Munisamy, V. M.; Reddy, D. Int J Chem Kinet 2006, 38, 202.
27. Hegmans, A.; Berners-Price, S. J.; Davies, M. S.; Thomas, D. S.; Humphreys, A. S.; Farrell, N. J Am Chem Soc 2004, 126, 2166.
28. Montero, E. I.; Benendetti, B. T.; Mangrum, J. B.; Oehlsen, M. J.; Qu, Y.; Farrell, N. P. Dalton Trans 2007, 4938.
29. Ruhayel, R. A.; Zgani, I.; Berners-Price, S. J.; Farrell, N. P. Dalton Trans 2011, 40, 4154, and references cited therein.
30. Ongoma, O. O; Jaganyi, D. Dalton Trans 2013, 42, 2724.
31. (a) Williams, J. W.; Qu, Y.; Bulluss, G. H.; Alvorado, E.; Farrell, N. P. Inorg Chem 2007, 46, 5820; (b) Fan, D.; Yang, X.; Ding, J.; Wang, X.; Zhang, S.; Mao, J; Lin, L.; Guo, Z. J. J Biol Inorg Chem 2007, 12, 655.
32. Ertürk, H.; Puchta, R.; van Eldik, R. Eur J Inorg Chem 2009 1331.
33. (a) Oehlsen, M. E.; Qu, Y.; Farrell, N. Inorg Chem 2003, 42, 5498; (b) Vacchina, V.; Torti, L.; Allievi, C.; Lobinski, R. J Anal At Spectrom 2003, 18, 884.
34. (a) Farrell, N. In: Platinum-Based Drugs in Cancer Therapy, Kelland, L. R.; Farrell, N., Eds.; Humana Press: Totowa, NJ, 2000, 321;(b) McGregor, T. D.; Balcarova, Z.; Qu, Y.; Tran, M. C.; Zaludova, R.; Brabec, V.; Farrell, N. J Biol Inorg Chem 1999, 77, 43; (c) Montero, E. I.; Zhang, J.; Moniodis, J. I.; Berners-Price, S. J.; Farrell, N. P. Chem Eur J 2010, 30, 9175.
35. (a) Summa, N.; Maigut, J.; Puchta, R.; van Eldik, R. Inorg Chem 2007, 46, 2094; (b) Hochreuther, S.; Puchta, R.; van Eldik, R. Inorg Chem 2011, 50, 12747; (c) Soldatović, T.; Jovanović, S.; Bugarčić, Ž. D.; van Eldik, R. Dalton Trans 2012, 41, 876.
36. Zhao, G.; Lin, H.; Zhu, S.; Chen, Y. Anti-Cancer Drug Des 1998, 13, 769.
37. Zhao, G.; Lin, H. Curr Med Anti-Cancer Agents 2005, 5, 137.
38. Perrin, D. D.; Armarego, W. L. F.; Perrin, D. R. Purification of Laboratory Chemicals, 2nd ed.; Pergamon, Oxford, UK, 1980.
39. Microcal™ Origin™ Version 7.5, Microcal Software, Inc., Northampton, MA, 1991-2003.
40. (a) De Faria, D. M.; Yoshida, M. I., et al. Polyhedron 2007, 26, 4525; (b) Marinho, M. V.; Yoshida, M. I.; Krambbrock, K.; Fernando, L.; De Oliveira, C.; Diniz, R.; Machado, F. C. J Mol Struct 2009, 923, 60.
41. Zhao, G.; Lin, H.; Zhu, S.; Sun, H.; Chen, Y. J Inorg Biochem 1998, 70, 219.
42. Hollis, L. S.; Amundsen, A. R.; Stern, E. W. J Med Chem 1989, 32, 128.
43. Bugarčić, Z. D.; Liehr, G.; van Eldik, R. J Chem Soc, Dalton Trans 2002, 951.
44. (a) Appleton, A. D.; Hall, J. R.; Ralph, S. F.; Thompson, C. S. M. Inorg Chem 1984, 23, 3521; (b) Romeo, R.; Cusumano, M. Inorg Chim Acta 1981, 49, 167.
45. Becke, A. D. J Chem Phys 1993, 98, 5648.
46. Hay, P. J.; Wadt, W. R. J Chem Phys 1985, 82, 299.
47. Zhao, G.; Hu, X. Trans Metal Chem 2004, 29, 607, and references cited therein.
48. Schiessl, W. C.; Summa, N.; Weber, C. F.; Gubo, S.; Ducker-Benfer, C.; Puchta, R.; van Eikema Hommes, N. J. R.; van Eldik, R. Z. Anorg Allg Chem 2005, 631, 2812.
49. Kemp, S.; Wheate, N. J.; Wang, S.; Collins, J. G.; Ralph, S. F.; Day, A. I.; Higgins, V. J.; Aldrich-Wright, J. R. J. Biol Inorg Chem 2007, 12, 969.
50. Summa, N.; Schiessl, W.; Puchta, R.; Van, Eikema Hommes N.; van Eldik, R. Inorg Chem 2006, 45, 2948.
51. Mambanda, A.; Jaganyi, D. Dalton Trans 2011, 40, 79.
52. (a) Pregonsin, P. S. Coord Chem Rev 1982, 33, 512; (b) Appleton, T. G.; Hall, J. R.; Ralph, S. F. Inorg Chem 1985, 24, 4685.
53. Cotton, F. A.; Wilkinson, G. Advanced Inorganic Chemistry, 2nd ed.; Interscience Publishers: New York, 1966, pp. 710, 754.
54. Jaganyi, D.; Tiba, F.; Munro, O. Q.; Perović, B.; Bugarčić, Ž. D. Dalton Trans 2006, 2943.
55. Iwadata, Y.; Kawamura, K.; Igarashi, K.; Mochinaga, J. J Phys Chem 1982, 86, 5206.
56. Pearson, R. G. J Am Chem Soc 1963, 85, 3533.
57. (a) Aŝperger, S., Chemical Kinetics and Inorganic Reaction Mechanisms, 2nd ed.; Kluwer/Plenum: New York, 2003; (b) Tobe, M. L.; Burges, J. Inorganic Reaction Mechanisms; Addison Wesley, Longman: London, 1999.
58. Atwood, J. D. Inorganic and Organometallic Reaction Mechanisms, 2nd ed.; Wiley-VCH: New York, 1997; pp. 43–61.